JACS
JOURNAL OF THE AMERICAN CHEMICAL SOCIETY
pubs.acs.org/JACS
Article

Single Ru(II) Ions on Ceria as a Highly Active Catalyst for Abatement of NO

Konstantin Khivantsev,* Nicholas R. Jaegers, Hristiyan A. Aleksandrov,* Inhak Song, Xavier Isidro Pereira-Hernandez, Mark H. Engelhard, Jinshu Tian, Linxiao Chen, Debora Motta Meira, Libor Kovarik, Georgi N. Vayssilov, Yong Wang,* and János Szanyi*

Cite This: J. Am. Chem. Soc. 2023, 145, 5029−5040
Read Online

ABSTRACT: Atom trapping leads to catalysts with atomically dispersed Ru_1O_5 sites on (100) facets of ceria, as identified by spectroscopy and DFT calculations. This is a new class of ceria-based materials with Ru properties drastically different from the known M/ceria materials. They show excellent activity in catalytic NO oxidation, a critical step that requires use of large loadings of expensive noble metals in diesel aftertreatment systems. Ru_1/CeO_2 is stable during continuous cycling, ramping, and cooling as well as the presence of moisture. Furthermore, Ru_1/CeO_2 shows very high NO_x storage properties due to formation of stable Ru−NO complexes as well as a high spill-over rate of NO_x onto CeO_2. Only ∼0.05 wt % of Ru is required for excellent NO_x storage. Ru_1O_5 sites exhibit much higher stability during calcination in air/steam up to 750 °C in contrast to RuO_2 nanoparticles. We clarify the location of Ru(II) ions on the ceria surface and experimentally identify the mechanism of NO storage and oxidation using DFT calculations and in situ DRIFTS/mass spectroscopy. Moreover, we show excellent reactivity of Ru_1/CeO_2 for NO reduction by CO at low temperatures: only 0.1−0.5 wt % of Ru is sufficient to achieve high activity. Modulation-excitation in situ infrared and XPS measurements reveal the individual elementary steps of NO reduction by CO on an atomically dispersed Ru ceria catalyst, highlighting unique properties of Ru_1/CeO_2 and its propensity to form oxygen vacancies/Ce^{+3} sites that are critical for NO reduction, even at low Ru loadings. Our study highlights the applicability of novel ceria-based single-atom catalysts to NO and CO abatement.

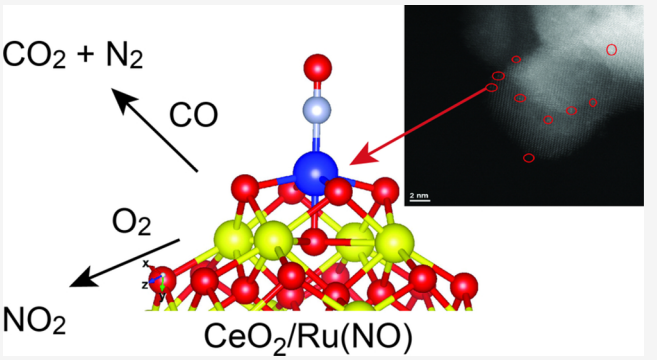

INTRODUCTION

Air pollution is one of the main issues to tackle in environmental science and catalysis.[1−3] Deteriorating air quality is directly related to toxic NO_x emissions, the majority of which are produced by vehicles exhaust. There clearly exists the urgent need to decrease emissions from engines and develop catalytic materials for NO_x abatement based on less expensive (noble) metals with improved atom economy.[4−19] NO oxidation is critical for environmental catalysis in diesel aftertreatment systems because NO_2 formation is important in lean NO_x reduction.[32−38] Furthermore, NO_2 facilitates ammonia selective catalytic reduction (SCR) (so-called "fast" SCR, with an ideal 1:1 ratio between NO and NO_2) and lean NO_x storage (in this case, NO must first be oxidized to NO_2 in order to be stored on LN traps materials). Best catalysts for NO oxidation typically contain a few wt % percent of expensive Pt and Pd.[32−38] Pt currently costs ∼1000 USD/ounce, whereas Pd costs ∼2600 USD/ounce (note that Pt is approximately ∼2 times heavier, so per molar basis, the price is only ∼1.3 higher for Pd than for Pt).

RESULTS AND DISCUSSION

Anchoring Pt, Pd, and Ru Ions to Ceria Support. In the recent decade, the so-called single-atom materials with efficient utilization of single metal atoms/ions have been introduced that may offer promising alternatives and unusual reactivities compared to traditional nanoparticle catalysts. For example, thermally stable atomically dispersed Pt materials on ceria have been prepared via the atom trapping approach at 800 °C.[28−31] We now extended this synthesis to Pd. We also turned our attention to another transition metal ruthenium, whose current price is ∼500 USD per ounce and whose molecular weight is similar to that of Pd and Rh (Rh, on the other hand, costs ∼15,000 USD per ounce, almost ∼30 times more on molar

Received: September 29, 2022
Published: February 22, 2023

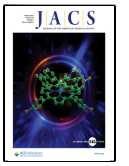

https://doi.org/10.1021/jacs.2c09873
J. Am. Chem. Soc. 2023, 145, 5029−5040

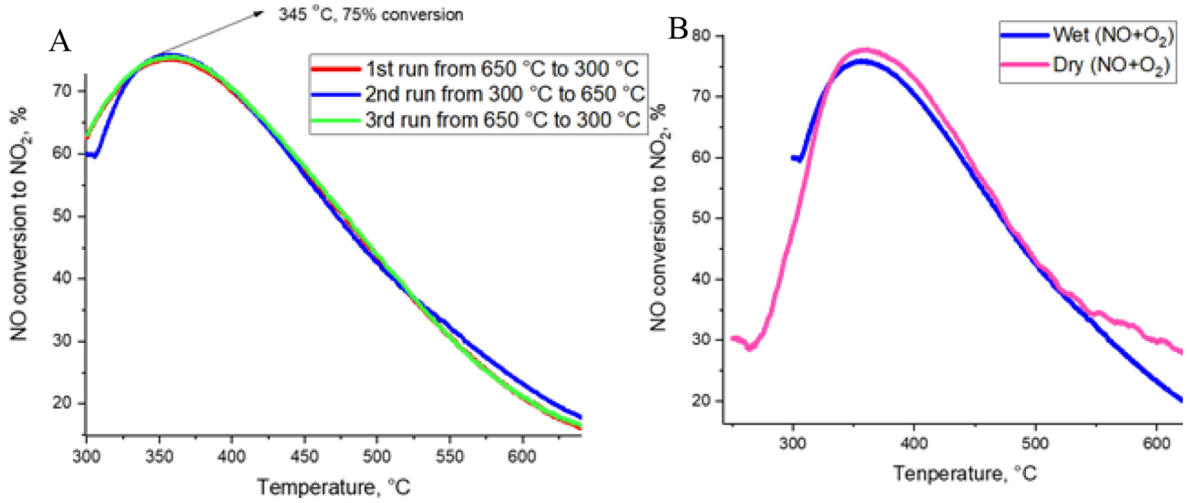

Figure 1. NO oxidation performance of (A) 0.5 wt % Ru/CeO_2 (3 continuous runs from 650 to 300, showing stable NO oxidation performance in the presence of ~3% H_2O, 120 mg catalyst, 470 ppm NO, 13% O_2, total flow 300 sscm/min, GHSV ~150 L/g*h). (B) Comparison of wet and dry NO oxidation on aged 0.5 wt % Ru/CeO_2 up to 650 °C (conditions are identical to A; dry experiments were carried out with the same NO and oxygen concentrations).

basis than Ru; Ru is approx ~4 times cheaper on per-molar basis than Pt and Pd). However, it is important to note that the general noble metal prices are volatile and are subject to supply/demand issues; the price trends generally hold within the last decade; therefore, it is also beneficial not only to utilize a less expensive metal but also to diversify the catalytic portfolio. Taking advantage of the atom trapping approach, we prepared isolated Pd, Pt, and Ru atoms on ceria in ~ equivalent molar amounts (atom loading per surface area of ceria) with 1 wt % Pt, 0.5 wt % Ru, and 0.5 wt % Pd on ceria. We note that ceria materials with isolated Ru(II) have not been prepared or characterized before as well as shown to have advantageous catalytic properties. We observed pronounced stabilization of the ceria surface area after heating at 800 °C, producing atomically dispersed M/Ceria materials as opposed to undoped ceria (Table S1), in agreement with previous studies.[42,72,73] Anchoring these ions onto ceria produces stable materials that can survive heating in air at 800 °C in agreement with our latest findings.[42] HAADF-STEM images of Pd, Pt, and Ru-supported ceria materials (Figures S1−S5) show crystalline ceria nanoparticles with no noble metal nanoparticles. In the case of Pt on ceria, we can identify single Pt atoms located on the surface of ceria (Figure S1−S5). However, in the case of Pd and Ru, although the contrast is poor, on sufficiently thin parts of ceria nanoparticles tilted slightly off the zone-axis (to decrease scattering from bright Ce atom columns), we could in fact identify single Ru atoms (shown by arrows on the surface of different ceria crystallites in Figure S5). In all three cases, EDS maps clearly reveal the presence of Pd, Pt, and Ru well-dispersed throughout the sample, further confirming our suggestion of atomic dispersion of the said metals on ceria.

NO Oxidation Performance of M_1/CeO_2. We tested these model single-atom materials for NO oxidation. Pt and Pd showed markedly lower NO oxidation activity than Ru (Figure S6): NO oxidation activity of single-atom Pt and Pd materials supported on redox-active supports has not been investigated to date. Typically employed catalysts include Pt and Pd oxide nanoparticles on different supports. We find that both Pt and Pd single atoms have markedly lower activity for NO oxidation, with Pd ions outperforming the Pt. 0.5 wt % Ru/ceria sample, in contrast, showed excellent NO oxidation activity in the steam-containing lean $NO/O_2/N_2$ stream (Figure 1).

The sample shows stable performance with little hysteresis going down, up, and then back down in temperature (from 650 to 300 °C). Activity maximum is observed at ~345 °C with ~75% conversion of NO. We also tested this sample in dry NO oxidation (Figure 1) and did not observe any prominent water influence on NO oxidation activity. Previously, only one study reported the activity of isolated metal atoms (Pt) on alumina for NO oxidation,[71] whereas the same authors found that Pd atoms on alumina were inactive.[72] We note that the activity of single-atom Ru, Pd, and Pt catalysts on ceria in terms of TOF is approximately an order of magnitude higher than the tabulated activity of Pt atoms and nanoparticles on alumina. Comparison with representative materials in terms of TOF can be found in Table S5. For comparison of NO oxidation activity on supported PGM and non-PGM nanoparticles, we refer the readers to the available reviews on this topic.[76]

We hypothesized that excellent NO oxidation activity only by single-atom Ru (and not Pt and Pd) is related to the presence of labile active lattice oxygen of ceria and the ability of Ru ions to form ruthenium nitrosyl complexes. If Ru−NO complexes indeed form, then, Ru ceria should be able not to just oxidize NO but also store NO at lower temperatures: this storage is critical during vehicle cold-start and idle operation when the temperatures of exhaust are lower (~100−120 °C) and no known catalyst can provide NO_x removal at this temperature. More specifically, Pd/zeolite formulations can store NO_x at low temperatures (~100 °C) and release them continuously at >180 °C.[7−27] Pd is expensive, and loadings of ~ at least 1−2 wt % are required to achieve optimal NO adsorption.

NO Storage Performance of M_1/CeO_2. We, therefore, performed NO adsorption experiments on single-atom M/Ceria materials. Pt and Pd store little NO, consistent with the lack of strong bond formation between NO and Pd(II)/Pt(II) on ceria (Figure S7).

https://doi.org/10.1021/jacs.2c09873
J. Am. Chem. Soc. 2023, 145, 5029−5040

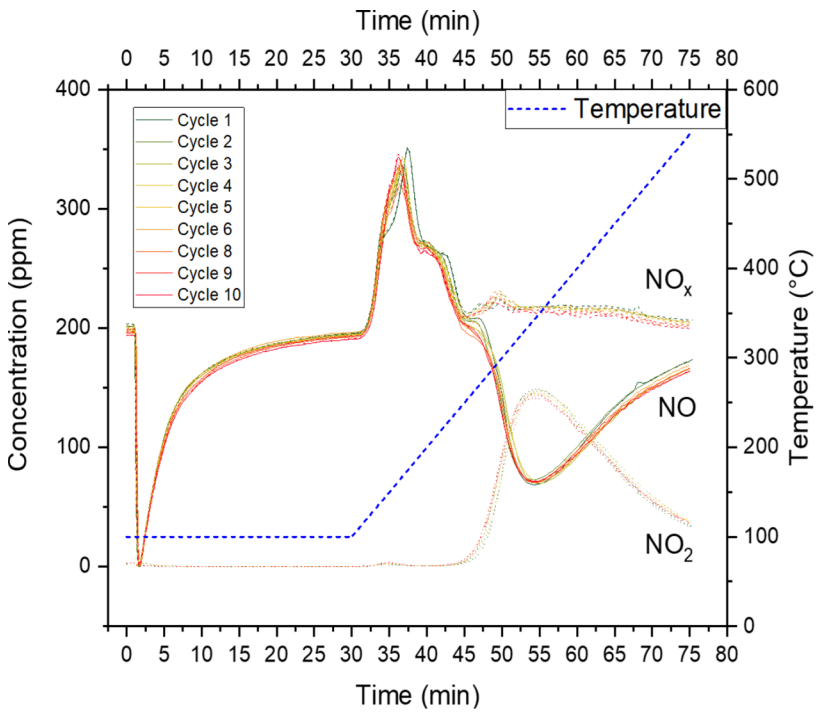

Cycle	μmol NOx	mol NOx/mol Ru
1	23.57	4.76
2	23.09	4.67
3	22.49	4.55
4	22.51	4.55
5	22.75	4.60
6	22.76	4.60
8	22.71	4.59
9	22.60	4.57
10	22.93	4.64

Figure 2. Performance and stability of 0.25 wt % Ru_1/CeO_2 during sequential cycles of low-temperature NO_x adsorption and NO oxidation. Gas composition was 200 ppm of NO, 2000 ppm CO, and 12% O_2, ~3% H_2O, balanced with N_2. 120 mg catalyst was used with GHSV ~150 L/g*h. Adsorption experiments were performed at 100 °C. The temperature ramp (10 °C/min) was started at a 30 min mark; up to 550 °C. NO_x storage is shown per 120 mg catalyst. On average, the stored NO_x amount is ~190 μmol/g.

We would like to note that formulations with Pd and Pt nanoparticles on ceria have been considered before for NO_x adsorption applications.[73−75] These formulations had high loadings of PGMs (>1 wt %) and were characterized by relatively low NO_x storage capacity (~20 μmol/g), whereas Pd/Zeolite formulations had maximum storage capacity <180 μmol/g in the best formulations for 2 wt % Pd/SSZ-13.

0.5 wt % Ru_1/CeO_2, however, showed very high NO uptake (Figures S7) with full consumption of NO (level ~0 ppm) even at 100 °C. Its performance is better than performance of Pd/SSZ-13 with Pd loading of 2 wt % (Figure S8). The NO/Ru ratio for this sample is ~2.7, showing that there must be another avenue of NO storage in addition to the Ru−NO complex (discussed further in the text). Hydrothermal aging at 750 °C in 10%$H_2O/O_2/N_2$ flow under simulated aging conditions does not lead to any appreciable loss of NO_x storage of 0.5 wt % Ru/ceria (Figure S9), consistent with high stability of Ru_1/CeO_2. This is notable considering well-known volatility of RuO_2 nanoparticles that typically form at higher Ru loading[68] (see discussion of our EXFAS data) just above ambient temperatures.[68] This hampered use of Ru/Ceria in typical NO reduction or oxidation formulations: these early formulations contained on the order of ~1−2 wt % Ru and thus contained a significant amount of RuO_2 nanoparticles (and significantly less isolated Ru sites; see our discussion of EXAFS data). Thus, isolating Ru ions as atomically dispersed species minimizes typical volatilization of extremely volatile RuO_x observed for supported RuO_x nanoparticles,[69] and Ru_1/CeO_2 represents an excellent NO oxidation catalyst (in the absence of Pt/Pd metals) with outstanding NO storage capacity at cold-start temperatures. We wondered if we could decrease the loading of Ru even further, while maintaining excellent NO adsorption properties and NO oxidation catalysis. We find that even at loading as low as 0.25 wt % Ru, full NO adsorption still can be achieved under simulated cold-start conditions with excellent NO oxidation activity (Figure 2). The sample shows stable NO adsorption, and NO oxidation activity was evaluated continuously over 10 cycles (Figures 2, S10). Furthermore, exposure of 0.25 wt % Ru_1/CeO_2 to SO_2 did not lead to destruction of NO adsorption and oxidation performance (Figure S34), highlighting the potential of single-atom materials to resist SO_2 poisoning typical for all ceria-supported oxidation catalysts. The total NO storage of 0.25 wt % Ru_1/CeO_2 is ~190 μmol/g, exceeding that of the best reported 2 wt % Pd/SSZ-13 materials: however, these Pd/SSZ-13 materials show degradation over cycling in the presence of CO, whereas Ru_1/CeO_2 does not. CO oxidation remains stable as well (Figures S9 and S10). This suggests that Ru/ceria materials with low Ru loadings are active CO oxidation catalysts even in the presence of NO and steam (NO is a known poison). For 0.25 wt % Ru/ceria, 90% CO conversion is achieved at 200 °C in the presence of steam and ~200 ppm NO at GHSV 150 L/g*h.

For all tested samples, ~100% of stored NO_x is released upon subsequent thermal ramp. This is underscored by the stability of NO adsorption/desorption within 10 cycles. Another important finding is that the NO/Ru ratio is ~2.7 for 0.5 wt % Ru_1, ~4.6 for 0.25 wt % Ru_1, and ~15 for 0.05 wt % Ru_1/CeO_2. (See detailed discussion in the manuscript further; Figure S30). Since spectroscopy confirms that 1 Ru ion can adsorb 1 NO, spill-over of NO to the ceria surface occurs and is promoted (catalyzed) by Ru presence as it does not occur on other noble metals supported on ceria based on the lack of NO storage. NO is initially stored as nitrites[52] on ceria after spill-over as evidenced by DRIFTS spectra in NO flow and the prominent ~1170 cm^{-1} nitrite band[52] (Figure

https://doi.org/10.1021/jacs.2c09873
J. Am. Chem. Soc. 2023, 145, 5029−5040

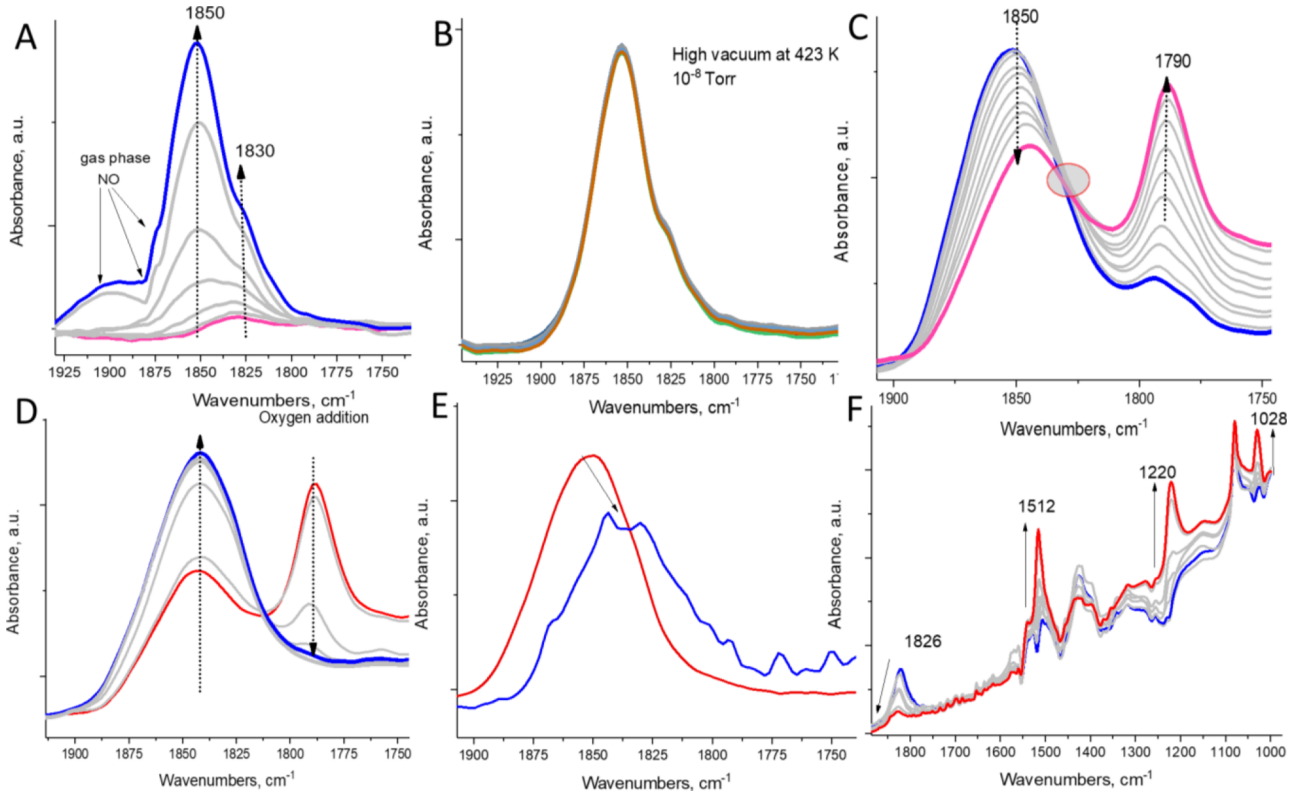

Figure 3. (A) NO adsorption (0.5 Torr equilibrium pressure) at 298 K. (B) High vacuum after NO adsorption at 423 K. (C) Heating Ru-NO from 150 to 220 °C. (D) Introducing O_2 at 220 °C after heating Ru−NO. (E) Water adsorption on the Ru-NO complex at 120 °C. (F) Ru−NO heated in the presence of O_2 + H_2O from 120 to 350 °C: Ru−NO diminishes and chelating nitrates form bands at 1512, 1220, and 1028 cm^{-1}.[53]

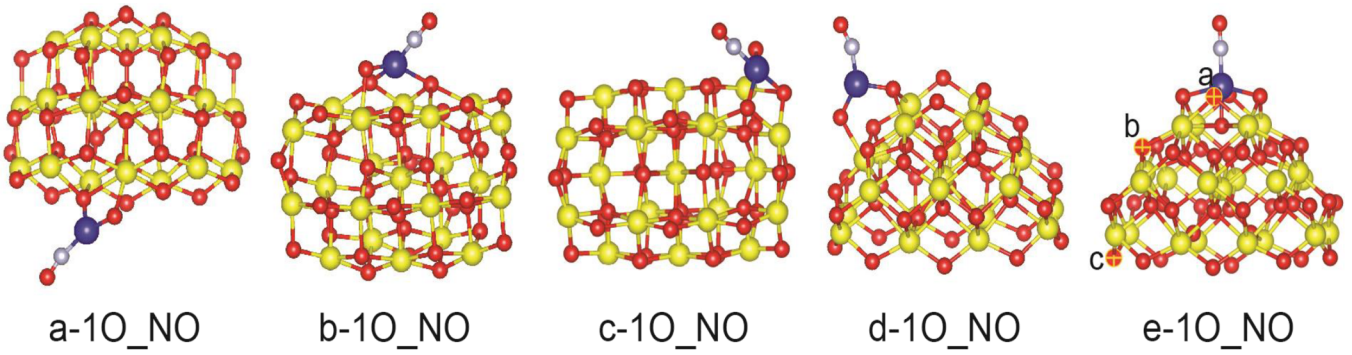

Figure 4. Optimized $RuO(NO)/Ce_{21}O_{42}$ structures. In the case of the e-1O_NO complex, the letters denote the O centers which are removed in order to obtain $RuO(NO)/Ce_{21}O_{41}$ structures. Color coding of atoms: Ce − yellow, O − red, Ru − dark blue, and N − gray. Additional snapshots of the $Ce_{21}O_{42}$ particle and its facets are shown in Figure S33.

S16). NO oxidation activity of 750 °C hydrothermally aged 0.25 wt % Ru_1/CeO_2 sample is comparable to the state-of-the-art industrial catalysts with ∼1 wt % Pd (and 0.5 wt % Pt) supported on ceria-aluminas (Figure S21). The TOF (normalized by total precious metal content) for this sample at 350 °C is ∼50 h^{-1} whereas it is at least ∼5 times lower for the state-of-the-art commercial catalyst (for which metallic or oxidized nanoparticles are considered to be active sites) tested under similar conditions and having >1 wt % (Pd and Pt) (Figure S5).

Infrared Spectroscopy Studies on NO Interaction with Ru_1/CeO_2. Ru-containing materials were studied for various catalytic processes[51,52] in the past, yet no spectroscopic investigation of single-atom Ru materials[43−46] was reported. A recent study[50] on catalytic CO_2 hydrogenation has reported that for 0.5 wt % Ru on ceria, dispersion of Ru nanoparticles into isolated Ru ions changed selectivity of hydrogenation from methane to CO.

We, therefore, studied CO and NO adsorption with infrared spectroscopy on 0.5 wt % Ru/ceria sample. CO adsorption (Figures S8 and S9) on the sample produces no metallic CO bands for Ru and reveals the presence of $Ru(II)(CO)_2$ and $Ru(II)(CO)_3$ complexes on the surface. Adsorption of NO produces a sharp band due to NO interaction with cationic Ru at ∼1850 cm^{-1} (Figure 3A).

This clearly indicates the formation of a Ru−NO complex, stable even under high vacuum of $\sim 10^{-8}$ Torr (Figure 3B).

Modeling of Ru_1/CeO_2 and Infrared Data. Recent advances in modeling ceria surface and metal-ceria interactions using state-of-the-art DFT methods can provide a molecular

https://doi.org/10.1021/jacs.2c09873
J. Am. Chem. Soc. 2023, 145, 5029−5040

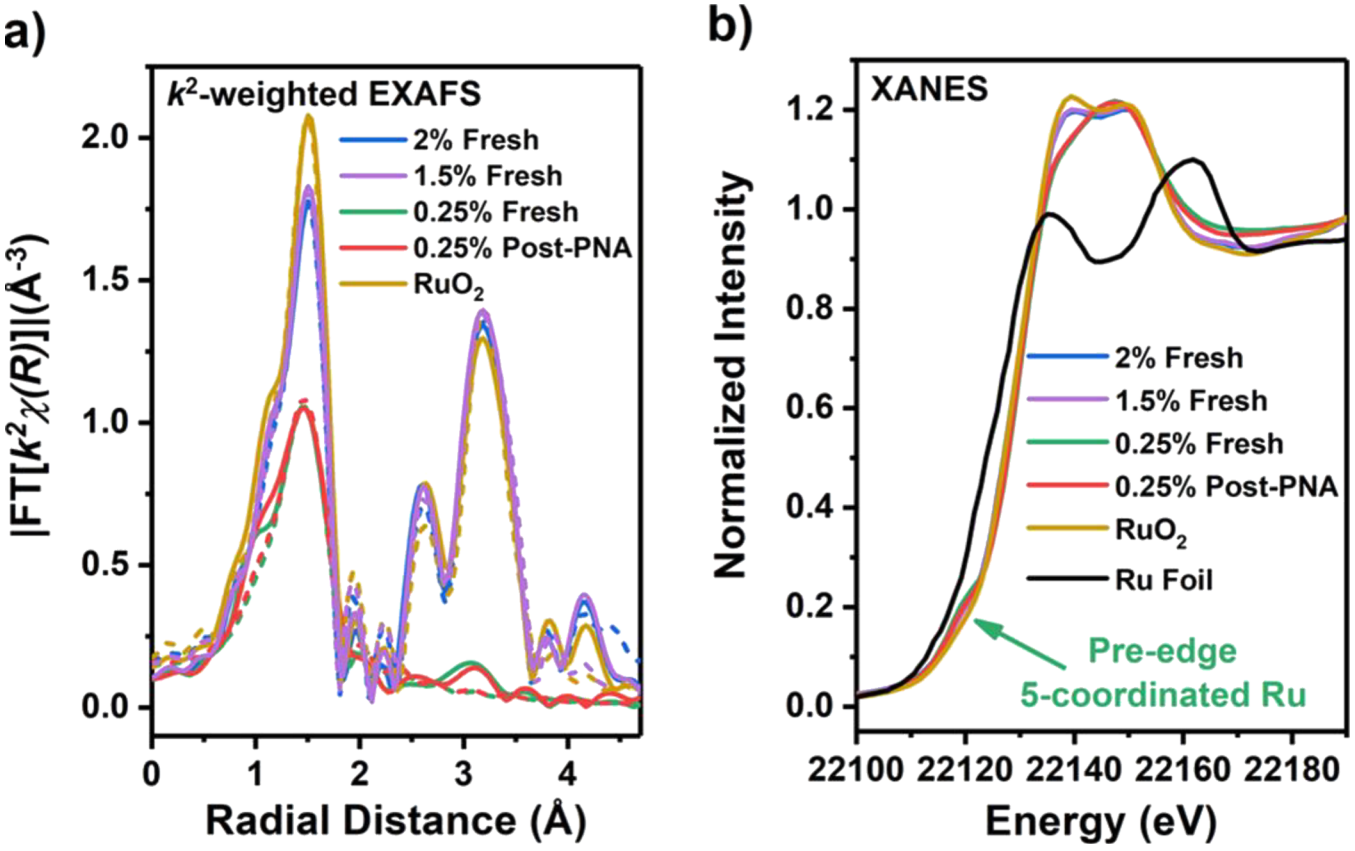

Figure 5. Ru K-edge XAS results on fresh 2% (blue), 1.5% (purple), 0.25% (green), and post-PNA 0.25% (red) samples. Panel a shows the EXAFS (*R*-space magnitude, best fittings shown as dashed curves, and fitting parameters listed in Table S4, *k*-space with fittings shown in Figure S28a). Panel b shows spectra in the XANES region. Results on RuO_2 and Ru foil are presented in yellow and black, respectively.

level insight into the precise nature and location of metal ions on ceria surfaces.[54−68] Therefore, we modeled NO complexes of Ru cations adsorbed in different locations on ceria. Five different $RuO(NO)/Ce_{21}O_{42}$ complexes were modeled (Figure 4, Table S2).

The most stable one, e-1O_NO, is obtained after adsorption of NO to the most stable $RuO/Ce_{21}O_{42}$ complex, e-1O (notation of the structures is as in ref 63).

In this complex, where the Ru center is in octahedral coordination at the small (100) facet of the $Ce_{21}O_{42}$ nanoparticle (Figure S33), NO donates an electron to a Ce^{4+} center; thus, the NO^+ ligand and a Ce^{3+} center are formed, while the formal charge of Ru remains +2. The other structures modeled are less stable by 1.42−2.91 eV, as the formal charge of Ru is +1, since the unpaired electron is transferred from NO to the Ru center. In the structures a-1O_NO and d-1O_NO, Ru is in triangular planar coordination, interacting with two O centers and the N atom from NO. The lowest N−O vibrational frequencies were calculated for these two structures, 1733 and 1763 cm^{-1}. Ru is in square-planar coordination in the structures b-1O_NO and c-1O_NO, which leads to higher N−O frequencies, 1799 and 1824 cm^{-1}. The highest frequency was calculated for the most stable structure, e-1O_NO, 1840 cm^{-1}, where Ru is in octahedral coordination (5 O and 1 N). This value is in excellent agreement with the experimental band at 1850 cm^{-1}. Thus, FTIR with the probe molecule NO combined with state-of-the-art DFT calculations precisely identify location of active isolated Ru^{+2} cations at the small (100) facets of ceria nanoparticles.

Upon temperature increase in the absence of oxygen (Figure 3C), this band begins to decline with a new band growing at ∼1790 cm^{-1} and a clear isosbestic point, indicating the simple stoichiometric transition of one Ru−NO complex into other. We suggest that this occurs due to oxygen-vacancy formation in the vicinity of the Ru atom: ON-Ru(*vac*)Ce. DFT calculations further corroborate this finding. To understand this process, we modeled structures with created O vacancy from $RuO(NO)/Ce_{21}O_{42}$ complexes (Table S2).

The most stable structure is e-1O_NO_vac_a, where an O center was removed from the first coordination sphere of the Ru cation. The creation of such O vacancy led to decrease of the N−O vibrational frequency from 1840 to 1788 cm^{-1} in excellent agreement with our experimental results. This is the first direct spectroscopic observation of the formation of an oxygen vacancy on ceria *in the direct vicinity of the metal ion next to ceria*. Further, as soon as we add oxygen to this system, the vacancy is healed and the NO adsorbed on Ru−O−Ce fully restores, further confirming our suggestion (Figure 3E). This NO band is robust under high vacuum at 150 °C and does not completely disappear even at 350 °C. In the presence of water, the NO band shifts to lower wavenumbers (Figure 3E), the phenomenon that has been previously described for Pd/SSZ-13 and Pd/ZSM-5 and due to co-coordination of water and NO to the same Pd ion.[47−49] We note, for example, that coordination of water to isoelectronic $Rh(I)(CO)_2$ and $Rh(I)(NO)_2$ complexes shifts the CO and NO bands to the lower wavenumbers. Simultaneously, in the presence of O_2/NO/H_2O in the IR cell, infrared spectra emerge after running this under PNA relevant temperatures (∼from 120 to 350 °C),

https://doi.org/10.1021/jacs.2c09873
J. Am. Chem. Soc. 2023, 145, 5029−5040

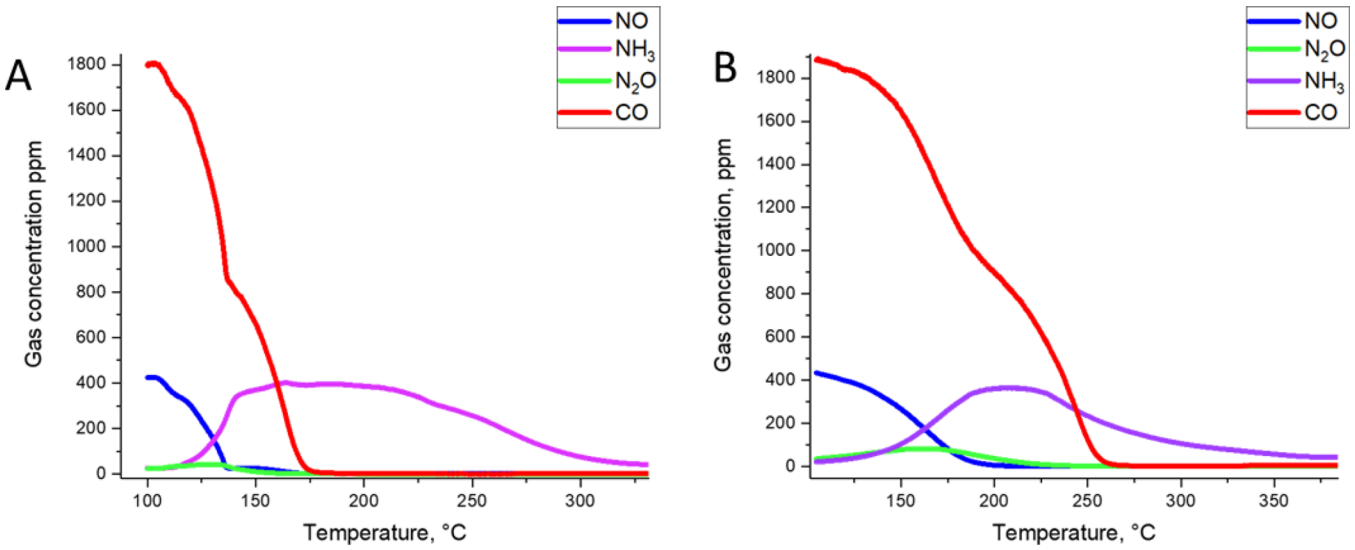

Figure 6. NO reduction performance of 0.5 wt % Ru/CeO_2 (A) and 0.1 wt % Ru/CeO_2 (B). 120 mg catalyst, 300 sscm/min total flow, GHSV ~150 L/G*h, 470 ppm NO, 1850 ppm CO, ~3% H_2O balanced in N_2. Performance of the 0.5 wt % Ru/CeO_2 sample under dry conditions is shown in Figure S16. Excellent performance of 0.5 and 0.1 wt % Ru/Ceria is comparable to recently reported state-of-the-art catalyst with 1 wt % Pd on Fe-doped ceria.[77]

showing the decrease of ruthenium nitrosyl complex and increase in chelating nitrate bands on the ceria surface (Figure 3F) as shown by studies of Hadjiivanov, Vayssilov, and co-workers.[53] Thus, ruthenium helps store NO both as a nitrosyl complex and allows NO_x to be stored on the ceria surface due to oxidation ability (as nitrites at low temperature and nitrates at higher temperatures in O_2 presence), explaining the high NO/Ru ratio which exceeds that of the NO/Pd ratio of Pd in zeolites.

EXAFS Studies on Ru/CeO_2 with Various Ru Loadings. Ru K-edge X-ray absorption spectroscopy (XAS) was performed on selected samples to probe the nuclearity, coordination environment, and electronic state of Ru. Figure 5a shows the k^2-weighted EXAFS in *R*-space magnitude (best fittings shown as dashed curves in the same colors). The EXAFS of 2% (blue) and 1.5% (purple) Ru/CeO_2 highly resembles that of RuO_2 (yellow), with strong scattering between 2 and 4 Å besides first-shell Ru−O scattering at ~1.5 Å. The data can be appropriately modeled by the combination of first-shell Ru−O, second-shell Ru−Ru, Ru−O, third-shell Ru−O, and Ru−O−Ru multiple scattering paths (Table S4) in the RuO_2 structure. Meanwhile, spectra in the XANES region is presented in Figure 5b, in which the two samples exhibit similar white-line intensity with RuO_2, indicating an Ru oxidation state close to +4. In addition, there is no pre-edge peak at ~22,120 eV in neither samples. This peak represents 1*s* → 4*d* electron transition, which is forbidden on 6-coordinated Ru, but is partially allowed with broken symmetry, that is, one missing ligand, as 5*p* components are mixed into 4*d* orbitals. Therefore, the absence of this peak suggests that the absolute majority of Ru on the two samples are 6-coordinated, consistent with the best EXAFS fitting model (Table S4) showing N(Ru−O) = 6.4 ± 0.8 and 6.3 ± 0.7 as well as the crystal structure of RuO_2. Overall, XAS suggests that on 2 and 1.5% Ru/CeO_2, Ru exist mainly as RuO_2 particles.

In contrast, the EXAFS of fresh 0.25% Ru/CeO_2 (green) has very low-intensity scattering between 2 and 4 Å. The response of the features in this range to changes in *k*-weight is similar with first-shell Ru−O scattering at ~1.5 Å, and much less sensitive than features in this range in 2%, 1.5% samples, and RuO_2 which have significant Ru−Ru contribution (Figures S28 and S29). This fact indicates that such features in 0.25% Ru/CeO_2 have much less high-*k* contribution than Ru−Ru scattering; that is, the main contributors are scatterers much lighter than Ru, in this case, O (see Figure S29b for potential paths).

The absence of Ru−Ru contribution to the EXAFS strongly indicates that Ru atoms on 0.25% Ru/CeO_2 are atomically dispersed. In the XANES region, the white-line intensity of the sample is between that of RuO_2 and Ru foil (black), implying the Ru oxidation state between +4 and 0, consistent with Ru(II) from DFT results. Furthermore, 0.25% Ru/CeO_2 shows an obvious ~22,120 eV pre-edge peak, indicating that a significant fraction of Ru is 5-coordinated, aligned well with the best model for its first-shell EXAFS having N(Ru−O) = 4.5 ± 0.8 (Table S4), and also consistent with DFT results. In fact, when using two first-shell Ru−O paths of different distance in the model, the bond length and coordination number ("2 O" models in Table S4) of both types of Ru−O *perfectly* match structures determined by DFT. We note that after fitting the EXAFS of 0.25% Ru/CeO_2 with only first-shell Ru−O, the residual oscillation is mostly in the low-*k* (<6 $Å^{-1}$) range (Figure S28a), further confirming that the scattering beyond the first shell has no Ru−Ru contribution. After using in PNA, neither the EXAFS nor the white-line intensity of 0.25% Ru/CeO_2 visibly changes (Figure 6, red compared to green), and the EXAFS still has no Ru−Ru contribution (Figures S28a, S29 and Table S4); that is, Ru remain as atomically dispersed Ru(II) post-PNA. The pre-edge peak in the XANES region diminishes slightly, suggesting that fewer Ru atoms are 5-coordinated, likely as a result of residual NO adsorption on Ru. In summary, XAS indicates that Ru on fresh 0.25% Ru/CeO_2 are single Ru(II) atoms, many of which are 5-coordinated, and they are stable after PNA. Thus, the coordination environment of Ru on ceria represents a new type of environment not observed for typically employed metal ions on ceria such as Rh, Pd, and Pt that are found on step edges and in the square-planar environment of oxygen, which is exemplified by

https://doi.org/10.1021/jacs.2c09873
J. Am. Chem. Soc. 2023, 145, 5029−5040

significantly different performance of Ru_1/CeO_2 for NO storage and oxidation compared to the typical M_1/CeO_2 and $M_{nanoparticle}$/Ceria catalysts that store >10 times less NO and that catalyze NO oxidation only when significant amounts of oxide nanoparticles are present.

Since we discovered that there are two mechanistic pathways of NO storage, we put vanishingly small amounts of Ru (0.05 wt %) on ceria and tested NO storage performance. Remarkably, this sample showed facile and excellent NO adsorption under industrially relevant conditions with the NO_x/Ru ratio approaching 15 (Figure S30; compared with 1 wt % Ru/Ceria in Figure S31). This, of course, means that NO_x is stored on the ceria surface, and the spill-over is facilitated even by the smallest amounts of Ru ions on the surface, revealing a new phenomenon in metal-ceria chemistry to improve interaction of ceria with NO species: this unprecedentedly high ability of Ru ions to function as a shuttle for NO_x molecules is believed to be important for various sensing, adsorption, and catalytic applications. This also allows us to disentangle the support-related storage and Ru-related storage: for 0.25 wt % Ru/ceria material, subtracting the baseline storage of NO_x on 0.05 wt % Ru/ceria yields approximately ∼1.4 molecules of NO per Ru atom (obviously, higher amounts of Ru facilitate even more spill-over of NO_x in addition to each Ru atom storing ∼1 NO molecule).

Understanding Mechanism of NO Oxidation on Ru_1/CeO_2 Using Spectroscopy and Modeling. We further investigated the NO oxidation mechanism of Ru_1/CeO_2 using combined DRIFTS and mass spectrometry. Figures S15−S20 shows *sequential* in situ DRIFTS and mass spectroscopy experiments that were performed.

We first performed NO adsorption in the DRIFTS flow-through cell, and the result agrees with static IR experiment: upon NO adsorption, the Ru−NO complex forms and surface nitrites form in great amounts. In the presence of oxygen, surface nitrites turn to surface nitrates at elevated temperatures. Only when the nitrates begin to decompose, mass spectroscopy TPD with in situ DRIFTS reveals that NO_2 begins to form (this holds true for a few continuous IR/TPD MS cycles performed) (Figures S18 and S19). We considered the NO oxidation on $RuO/Ce_{21}O_{42}$ complexes (Table S3 and Figure S27), considering the most stable positions for RuO species on both types of facets (100 and 111) on the $Ce_{21}O_{42}$ nanoparticle, e-1O and c-1O structures, respectively. This process includes four reaction steps: (1) oxidation of Ru species to RuO; (2) adsorption of NO to $RuO/Ce_{21}O_{42}$; (3) NO oxidation to NO_2 on Ru, as in the case of the c-1O_NO complex; the oxidation was considered from that additionally adsorbed in the first reaction step O center, while in the e-1O_NO complex, the oxidation was done by a O center from the (100) facet; and (4) NO_2 desorption from $Ru/Ce_{21}O_{42}$. The first two adsorption steps are strongly exothermic, while the oxidation and desorption are strongly endothermic. The rate-limiting step appears to be NO oxidation, as the barriers are as high as 182 and 249 kJ/mol, respectively, on c-1O and e-1O sites. However, if all contributions to the enthalpy as well as the entropy are taken into account at a temperature of 623 K, the corresponding Gibbs free barriers become 154 and 200 kJ/mol. The former barrier seems to be operative at 623 K, as the calculated kinetic constant is 1.58 s^{-1} (pre-exponential factor of the Eyring equation was taken to be 1), which corresponds to a half-life $T1/2$ of ∼0.44 s. The NO_2 desorption is strongly endothermic, but when the entropy contribution is considered, the endothermicity of the process is reduced by ∼150 kJ/mol; as in the case of the e-1O complex, it becomes even exothermic. This corresponds very well with our DRIFTS/mass spectroscopy data showing that NO association with interfacial Ru−O−Ce oxygen as well as nitrate decomposition steps are the legitimate pathways of NO_2 formation. The real rate constant at 623 K corresponds to ∼0.015 s^{-1} per Ru site (∼50 h^{-1}). The significantly lower number actually also suggests that not all sites participate in catalysis. Furthermore, it exceeds the TOF estimated for the most effective bimetallic and monometallic Pt and PtPd catalysts by at least ∼5 times.[68] For active catalytic formulations tested under similar industrially relevant conditions, normalization of the TOF frequencies in the desired temperature range per total precious metal amount yields TOF frequencies on the order of ∼6 h^{-1}. It is important to note that the industrial formulations always include significant amounts of Pd and Pt (total loading ∼1.5−2 wt % typically). Therefore, Ru−O−Ce sites of single-atom Ru/ceria catalysts are very active for NO oxidation. However, the corresponding single-atom Pt(Pd)−O−Ce is a poor NO (and CO, for Pt[27−31]) oxidation catalyst due to its inability to make Pt and Pd form a stable metal-NO bond that would ensure coverage of NO, when the interfacial O removal from M−O−Ce sites becomes favorable, as well as a spill-over of NO species onto the ceria support as nitrates. Thus, Ru_1/CeO_2 stands out as the only known ceria-supported material able to form thermally stable Ru−NO complexes.

Activity of Ru_1/CeO_2 in NO Reduction by Carbon Monoxide. To confirm the versatility of Ru/ceria materials for NO_x abatement catalysis, we now turn our attention to another challenging reaction for gasoline engines called NO reduction. TWC materials should perform catalytic removal of NO_x in the presence of CO and water vapor under stoichiometric conditions.[39−42] We recently discovered that isolated Rh(I) ions on ceria can perform low temperature NO reduction with CO[42] effectively. We, therefore, wondered if isolated Ru(II) ions could also perform NO reduction with CO.[69−71] 0.5 wt % Ru/ceria sample is excellent for NO reduction by CO under dry conditions.[77] Addition of water to the stream, in fact, does not lead to activity deterioration (Figures 6, S21): in this case, ammonia production is observed in significant amounts due to Ru/ceria being an excellent water-gas-shift catalyst.[42] Decreasing Ru loading to 0.1 wt % also produces an active NO reduction catalyst, with excellent activity and full NO conversion ∼185 °C (Figure 6). Thus, Ru_1/CeO_2 is an active catalyst for NO reduction by CO even at low Ru loading. TOF per Ru atoms ∼370 h^{-1} at 185 °C. In our recent paper,[42] we showed the first example of the single-atom Rh ceria-supported catalyst for NO reduction by CO, very active at low temperatures. Under similar GHSV and testing conditions, Rh single atoms were active catalysts with TOF ∼300 h^{-1} at ∼130 °C. Although Ru(II) ions are marginally less active than Rh, the impressive catalytic performance is still achieved at low temperature with a significantly cheaper metal. In fact, its performance is comparable with recent reports for state-of-the-art 1 wt % Pd catalyst on Fe-doped ceria[77] but on undoped ceria with less PGM (2 to 10 times) and significantly less expensive PGM. Based on our preliminary data,[42] we previously suggested a possible catalytic mechanism for Rh_1/CeO_2.

https://doi.org/10.1021/jacs.2c09873
J. Am. Chem. Soc. 2023, 145, 5029−5040

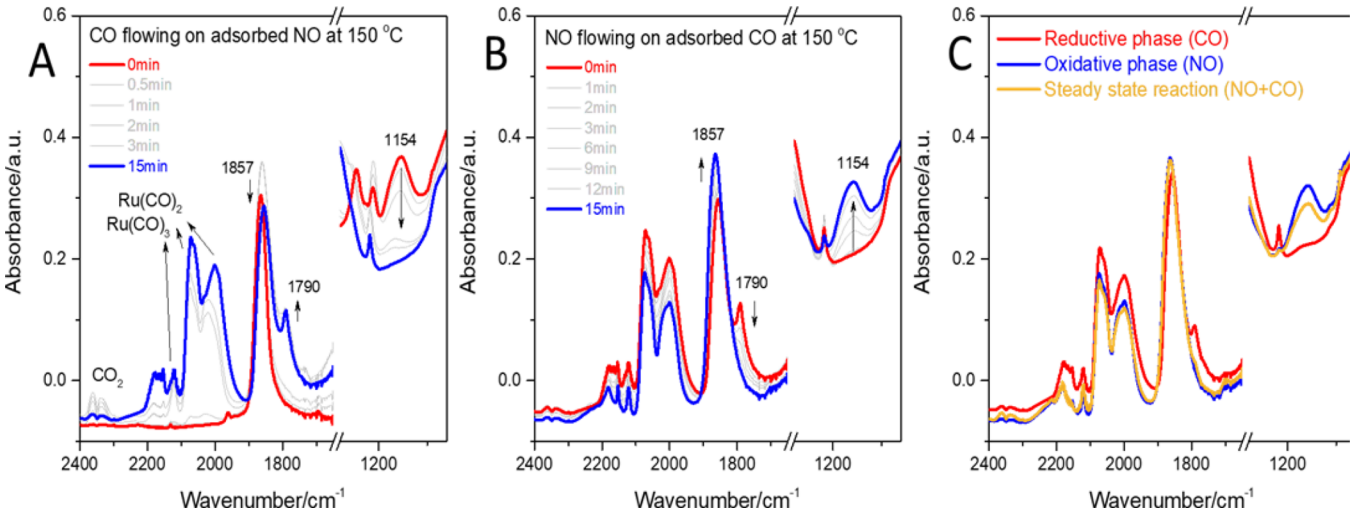

Figure 7. In situ DRIFTS on 0.25 wt % Ru_1/CeO_2. (A) Exposure to CO (2500 ppm) of NO-saturated sample (saturated with 500 ppm NO flow for 30 min and then purged with He at 150 °C before exposure to CO). (B) Subsequent exposure to NO flow after CO at 150 °C. (C) Comparison of the Ru_1/CeO_2 during exposure to 2500 ppm CO in the flow ("reductive phase"), 500 ppm exposure to NO in the flow ("oxidative phase"), and (500 ppm NO + 25,000 ppm CO) exposure in the flow (steady state reaction; in the DRIFTS cell NO conversion ∼30% under these conditions) at 150 °C.

The mechanistic aspects of NO reduction by CO have always been elusive because the typical materials used for this reaction contain poorly defined structures (nanoparticles): this made direct correlation of reactivity to structure for NO reduction very problematic. With well-defined single Ru(II) ions on ceria that are present as uniform isolated sites on the redox-active surface, we have a unique opportunity to identify the mechanism of NO reduction by CO using in situ and modulation-excitation infrared spectroscopy under the real flow-through conditions.

Pinpointing the Mechanism of NO Reduction by CO on Ru_1/CeO_2. In order to do so, we employed the modulation-excitation DRIFTS approach[78−80] in our infrared measurements: in short, at a temperature where (NO + CO) conversion occurs (150 °C), NO or CO flow pulses were applied to the system in antiphase for three consecutive cycles. The bands that appear/disappear in the antiphase during these treatments indicate the appearance/consumption of the true catalytically active intermediates. Additionally, we performed in situ DRIFTS with (NO + CO) flow at the same temperature (Figures 7, S22−S25).

During NO flow (∼500 ppm) at the 150 °C Ru−NO band at ∼1850 cm^{-1} appears, as well as nitrite bands associated with ceria at ∼1160 cm^{-1}. NO was then stopped, and CO flow started (2500 ppm) (Figure 7). Very notable changes were observed: nitrite band quickly decreased; simultaneously, the Ce−O−Ru−NO band (1860 cm^{-1}) decreased with the concomitant evolution of the Ce-vacancy-Ru−NO band (1790 cm^{-1}). Furthermore, the carbonate bands, easily attributable to poly- and monodentate carbonates, appeared (due to CO_2 evolution; some of which re-adsorbs on the surface at 150 °C).

We then followed with NO treatment: NO treatment leads to the fast restoration of the Ru−NO band with the simultaneous healing of oxygen vacancy; at the same time, nitrite bands re-appear at 1160 cm^{-1}. Repetition of these NO-CO modulation-excitation cycles three times allows to observe the phases that appear/disappear (respond dynamically during each cycle; Figures S16−S20). The ones that are in the anti-phase correspond to the active catalytic intermediates of the NO reduction by CO: indeed, during CO reduction: nitrites bands and Ru−NO bands are consumed with the formation of the oxygen vacancy between Ru(vacancy)Ce and CO_2 (carbonates). Treatment with NO leads to re-filling of the oxygen vacancy with oxygen from NO and restoration of nitrite bands. We previously suggested based on ex-situ measurements that for Rh_1/CeO_2, CO reduces Rh(III) to Rh(I) (which we suggested to be the rate-limiting step of this reaction) with the following re-oxidation of Rh(I) with NO to Rh(III). Now, we show generally that we observe similar chemistry in situ: but in this case, we prove the importance and direct participation of the oxygen vacancy between Ru and Ce in catalysis: this vacancy is created by the process (R1−R5):

$$CO - Ru - O - Ce \rightarrow CO_2 + Ru(vac)\ Ce \quad (R1)$$

$$Ru(vac)\ Ce + 2NO \rightarrow NO - Ru(vac)\ Ce - NO \rightarrow Ru(N_2O_2)Ce \rightarrow Ru - O - Ce + N_2O \quad (R2)$$

$$NO - Ru - O - Ce \rightarrow Ru(vac)\ Ce - NO_2 \quad (R3)$$

$$CO + Ru(vac)\ Ce - NO_2 \rightarrow CO - Ru\ Ce - NO_2 \rightarrow CO_2 + Ru(vac)Ce - NO + NO \rightarrow Ru\ (N_2O_2)\ Ce \rightarrow Ru - O - Ce + N_2O \quad (R4)$$

$$Ru(vac)Ce + N_2O \rightarrow O{=}N{=}N - Ru(vac)Ce \rightarrow N_2 + Ru - O - Ce \quad (R5)$$

The observation of the surface species during (NO + CO) flow over the Ru/ceria sample in the DRIFTS cell (∼30% NO conversion based on Mass-Spec data) and comparison with the states during NO and CO flows (Figure 7) allow us to conclude that during the reaction, the surface remains mostly "oxidized". This can be rationalized by the fact that the rate-limiting step of NO reduction is the removal of O between

https://doi.org/10.1021/jacs.2c09873
J. Am. Chem. Soc. 2023, 145, 5029−5040

Ru−O−Ce by CO with the formation of CO_2: the subsequent steps (re-filling of the oxygen vacancy by NO) occur much faster and during NO + CO flow, we find basically mostly oxidized surface. We emphasized earlier in the manuscript the remarkable lability of oxygens of ceria in Ru_1/CeO_2. This holds even for ultra-low Ru loadings of 0.05 wt %, which we further prove with XPS (Figure S32; the presence of only 0.05 wt % Ru is sufficient to observe the greatly increased surface reducibility of Ce after CO or H_2 treatments under mild conditions.

To further show the benefit of ultra-low Ru amounts on TWC, we performed NO reduction catalysis on 0.2 wt % Rh materials supported on ceria in the presence and absence of 0.05 wt % Ru (Figure S35). We tested these catalysts fresh and after harsh aging (950 °C, 10% H_2O/N_2 flow, 5 h). Addition of such small amounts of Ru resulted in shift of NO and CO conversion curves to lower temperatures both for fresh and aged catalysts by at least 25 °C, highlighting benefits of ultra-low Ru amounts for a typical Rh TWC catalyst.

Thus, the in situ dynamic NO/CO experiment allowed us to clarify the mechanism as well as slow/fast steps of NO/CO reaction on atomically dispersed metal catalysts for the first time.

CONCLUSIONS

In summary, we show brand new aspects of adsorptive and catalytic chemistry of ceria on the basis of well-defined Ru_1/CeO_2 catalysts. They show promising performance for challenging NO_x pollutant abatement even at low metal loadings. We elucidate the location of active Ru(II) cations on the surface of ceria and provide molecular level understanding of the mechanism of NO oxidation, low-temperature NO storage, and NO reduction by CO on these materials, paving the way for further developments in the important field of ceria-supported noble metals.

ASSOCIATED CONTENT

Supporting Information

The Supporting Information is available free of charge at https://pubs.acs.org/doi/10.1021/jacs.2c09873.

Materials and methods, HAADF-STEM images and corresponding EDS maps, adsorption and catalytic data, DFT optimized structures and DFT data, EXAFS analysis data, and infrared spectroscopy data (PDF)

AUTHOR INFORMATION

Corresponding Authors

Konstantin Khivantsev − *Institute for Integrated Catalysis, Pacific Northwest National Laboratory, Richland, Washington 99352, United States;* orcid.org/0000-0002-4810-586X; Email: Konstantin.Khivantsev@pnnl.gov

Hristiyan A. Aleksandrov − *Faculty of Chemistry and Pharmacy, Sofia University "St. Kliment Ohridski", 1126 Sofia, Bulgaria;* orcid.org/0000-0001-8311-5193; Email: Haa@chem.uni-sofia.bg

Yong Wang − *Institute for Integrated Catalysis, Pacific Northwest National Laboratory, Richland, Washington 99352, United States;* orcid.org/0000-0002-8460-7410; Email: Yong.Wang@pnnl.gov

János Szanyi − *Institute for Integrated Catalysis, Pacific Northwest National Laboratory, Richland, Washington 99352, United States;* orcid.org/0000-0002-8442-5465; Email: Janos.Szanyi@pnnl.gov

Authors

Nicholas R. Jaegers − *Institute for Integrated Catalysis, Pacific Northwest National Laboratory, Richland, Washington 99352, United States*

Inhak Song − *Institute for Integrated Catalysis, Pacific Northwest National Laboratory, Richland, Washington 99352, United States*

Xavier Isidro Pereira-Hernandez − *Institute for Integrated Catalysis, Pacific Northwest National Laboratory, Richland, Washington 99352, United States*

Mark H. Engelhard − *Institute for Integrated Catalysis, Pacific Northwest National Laboratory, Richland, Washington 99352, United States;* orcid.org/0000-0002-5543-0812

Jinshu Tian − *Institute for Integrated Catalysis, Pacific Northwest National Laboratory, Richland, Washington 99352, United States*

Linxiao Chen − *Institute for Integrated Catalysis, Pacific Northwest National Laboratory, Richland, Washington 99352, United States*

Debora Motta Meira − *Canadian Light Source: Canadian Light Source Inc., Saskatoon, Saskatchewan S7N 2V3, Canada;* orcid.org/0000-0002-7529-2736

Libor Kovarik − *Institute for Integrated Catalysis, Pacific Northwest National Laboratory, Richland, Washington 99352, United States*

Georgi N. Vayssilov − *Faculty of Chemistry and Pharmacy, Sofia University "St. Kliment Ohridski", 1126 Sofia, Bulgaria;* orcid.org/0000-0002-5185-8002

Complete contact information is available at: https://pubs.acs.org/10.1021/jacs.2c09873

Notes

The authors declare no competing financial interest.

ACKNOWLEDGMENTS

The research at Pacific Northwest National Laboratory (PNNL) was supported by the U.S. Department of Energy, Energy Efficiency and Renewable Energy, Vehicle Technology Office. Experiments were conducted in the Environmental Molecular Sciences Laboratory (EMSL), a national scientific user facility sponsored by the Department of Energy's Office of Biological and Environmental Research at PNNL. PNNL is a multiprogram national laboratory operated for the Department of Energy (DOE) by Battelle Memorial Institute under Contract DE-AC06-76RL01830. We acknowledge the support of CLEERS (Crosscut Lean Exhaust Emissions Reduction Simulations). CLEERS is an initiative funded by the U.S. Department of Energy (DOE) Vehicle Technologies Office to support the development of accurate tools for use in the design, calibration, and control of next generation engine/emissions control systems that maximize efficiency, while complying with emission regulations. HAA gratefully acknowledges the support by Bulgarian National Science Fund (project DN-19/2). GNV acknowledges the support of the project EXTREME, funded by the Bulgarian Ministry of Education and Science, D01-76/30.03.2021 through the program "European Scientific Networks". Computational resources are provided by Avitohol supercomputer, supported by Bulgarian Ministry of Education and Science via National Roadmap for Research Infrastructures. The previous version of this paper

was uploaded on the pre-print server ChemRxiv on July 23, 2020: DOI: 10.26434/chemrxiv.12692264.v1.

REFERENCES

(1) Holgate, S. T. 'Every breath we take: the lifelong impact of air pollution' – a call for action. *Clin. Med.* **2017**, *17*, 8–12.
(2) Jaegers, N. R.; Lai, J. K.; He, Y.; Walter, E.; Dixon, D. A.; Vasiliu, M.; Chen, Y.; Wang, C. M.; Hu, M. Y.; Mueller, K. T.; Wachs, I. E.; Wang, Y.; Hu, J. Z. Mechanism by which Tungsten Oxide Promotes the Activity of Supported V2O5/TiO2 Catalysts for NOX Abatement: Structural Effects Revealed by 51V MAS NMR Spectroscopy. *Angew. Chem., Int. Ed.* **2019**, *131*, 12739–12746.
(3) Kwak, J.-H.; Tonkyn, R. G.; Kim, D. H.; Szanyi, J.; Peden, C.; Catal, J. Excellent activity and selectivity of Cu-SSZ-13 in the selective catalytic reduction of NOx with NH3. *J. Catal.* **2010**, *275*, 187–190.
(4) Bull, I., Moini, A.; Koermer, G.; Patchett, J.; Jaglowski, W.; Roth, S., Zeolite catalyst with improved NOX reduction in SCR, US Patent US20070134146A1, 2010.
(5) Zones, S. I., Zeolite SSZ-13 and its method of preparation, US Patent 4 544 538, 1985.
(6) Seiyama, T.; Arakawa, T.; Matsuda, T.; Yamazoe, N.; Takita, Y. Catalytic reduction of nitric oxide with ammonia over metal ion-exchanged Y zeolites. *Chem. Lett.* **1975**, *4*, 781–784.
(7) Chen, H.-Y.; Collier, J. E.; Liu, D.; Mantarosie, L.; Durán, D.; Novák, V.; Rajaram, R.; Thompsett, D. Low Temperature NO Storage of Zeolite Supported Pd for Low Temperature Diesel Engine Emission Control. *Catal. Lett.* **2016**, *146*, 1706–1711.
(8) Khivantsev, K.; Jaegers, N. R.; Kovarik, L.; Hanson, J. C.; Tao, F. F.; Tang, Y.; Zhang, X.; Koleva, I.; Aleksandrov, H. A.; Vayssilov, G. N.; Wang, Y.; Gao, F.; Szanyi, J. Achieving atomic dispersion of highly loaded transition metals in small-pore zeolite SSZ-13. *Angew. Chem., Int. Ed.* **2018**, *130*, 16914–16919.
(9) Khivantsev, K.; Jaegers, N. R.; Kovarik, L.; Prodinger, S.; Derewinski, M. A.; Wang, Y.; Gao, F.; Szanyi, J. Palladium/Beta zeolite passive NOx adsorbers (PNA): Clarification of PNA chemistry and the effects of CO and zeolite crystallite size on PNA performance. *Appl. Catal. A. Gen.* **2019**, *569*, 141–148.
(10) Khivantsev, K.; Jaegers, N. R.; Koleva, I. Z.; Aleksandrov, H. A.; Kovarik, L.; Engelhard, M.; Gao, F.; Wang, Y.; Vayssilov, G. N.; Szanyi, J. Stabilization of Super Electrophilic Pd+2 Cations in Small-Pore SSZ-13 Zeolite. *J. Phys. Chem. C* **2020**, *124*, 309–321.
(11) Khivantsev, K.; Gao, F.; Kovarik, L.; Wang, Y.; Szanyi, J. Molecular level understanding of how oxygen and carbon monoxide improve NO x storage in palladium/SSZ-13 passive NO x adsorbers: The role of NO+ and Pd (II)(CO)(NO) species. *J. Phys. Chem. C* **2018**, *122*, 10820–10827.
(12) Moliner, M.; Corma, A. From metal-supported oxides to well-defined metal site zeolites: the next generation of passive NOx adsorbers for low-temperature control of emissions from diesel engines. *React. Chem. Eng.* **2019**, *4*, 223–234.
(13) Khivantsev, K.; Jaegers, N. R.; Kovarik, L.; Hu, J. Z.; Gao, F.; Wang, Y.; Szanyi, J. Palladium/zeolite low temperature passive NOx adsorbers (PNA): structure-adsorption property relationships for hydrothermally aged PNA materials. *Emiss. Control Sci. Technol.* **2020**, *6*, 126–138.
(14) Bello, E.; Margarit, V. J.; Gallego, E. M.; Schuetze, F.; Hengst, C.; Corma, A.; Moliner, M. Deactivation and regeneration studies on Pd-containing medium pore zeolites as passive NOx adsorbers (PNAs) in cold-start applications. *Microporous Mesoporous Mater.* **2020**, *302*, No. 110222.
(15) Khivantsev, K.; Jaegers, N. R.; Kovarik, L.; Wang, M.; Hu, J. Z.; Wang, Y.; Derewinski, M. A.; Szanyi, J. The Superior Hydrothermal Stability of Pd/SSZ-39 in Low Temperature Passive NOx Adsorption (PNA) and Methane Combustion. *Appl. Catal., B* **2021**, *280*, No. 119449.
(16) Rajaram, R.; Chen, H.-Y.; Liu, D., Passive NOx adsorber, US Patent US20150158019A1, 2015.
(17) Song, I.; Khivantsev, K.; Wu, Y.; Bowden, M.; Wang, Y.; Szanyi, J. Unusual water-assisted NO adsorption over Pd/FER calcined at high temperatures: The effect of cation migration. *Appl. Catal., B* **2022**, *318*, No. 121810.
(18) Song, I.; Khivantsev, K.; Wang, Y.; Szanyi, J. Elucidating the Role of CO in the NO Storage Mechanism on Pd/SSZ-13 with in Situ DRIFTS. *J. Phys. Chem. C* **2022**, *126*, 1439–1449.
(19) Khivantsev, K.; Szanyi, J.; Jaegers, N. R.; Kovarik, L.; Gao, F.; Wang, Y. High-capacity, low-temperature, passive NOx and CO adsorbers and methods for making same. US Patent 11,071,966, 2021.
(20) Lee, J.; Lim, T. H.; Lee, E.; Kim, D. H. Promoting the Methane Oxidation on Pd/CeO2 Catalyst by Increasing the Surface Oxygen Mobility via Defect Engineering. *ChemCatChem* **2021**, *13*, 3706–3712.
(21) Lee, J.; Kim, Y.; Hwang, S.; Lee, E.; Lee, H.; Kim, C. H.; Kim, D. H. Deactivation of Pd/Zeolites passive NOx adsorber induced by NO and H2O: Comparative study of Pd/ZSM-5 and Pd/SSZ-13. *Catal. Today* **2021**, *360*, 350–355.
(22) Heo, I.; You, Y. W.; Lee, J. H.; Schmieg, S. J.; Yoon, D. Y.; Kim, C. H. Urealess NOx Reduction by Carbon Monoxide in Simulated Lean-Burn Exhausts. *Environ. Sci. Technol.* **2020**, *54*, 8344–8351.
(23) Ryou, Y. S.; Lee, J.; Cho, S. J.; Lee, H.; Kim, C. H.; Kim, D. Activation of Pd/SSZ-13 catalyst by hydrothermal aging treatment in passive NO adsorption performance at low temperature for cold start application. *Appl. Catal. B Environ.* **2017**, *212*, 140–149.
(24) Ryou, Y. S.; Lee, J.; Lee, H.; Kim, C. H.; Kim, D. H. Effect of various activation conditions on the low temperature NO adsorption performance of Pd/SSZ-13 passive NOx adsorber, Comparative study of the mobility of Pd species in SSZ-13 and ZSM-5, and its implication for their activity as passive NOx adsorbers (PNAs) after hydro-thermal aging. *Catal. Today* **2019**, *320*, 175–180.
(25) Lee, J.; Ryou, Y.; Hwang, S.; Kim, Y.; Cho, S. J.; Lee, H.; Kim, C. H.; Kim, D. H. Comparative study of the mobility of Pd species in SSZ-13 and ZSM-5, and its implication for their activity as passive NOx adsorbers (PNAs) after hydro-thermal aging. *Catal. Sci. Technol.* **2019**, *9*, 163–173.
(26) Kim, Y.; Hwang, S.; Lee, J.; Ryou, Y. S.; Lee, H.; Kim, C. H.; Kim, D. H. Comparison of NOx Adsorption/Desorption Behaviors over Pd/CeO2 and Pd/SSZ-13 as Passive NOx Adsorbers for Cold Start Application. *Emiss. Control Sci. Technol.* **2019**, *5*, 172–182.
(27) Khivantsev, K.; Wei, X.; Kovarik, L.; Jaegers, N. R.; Walter, E. D.; Tran, P.; Wang, Y.; Szanyi, J. Palladium/Ferrierite versus Palladium/SSZ-13 Passive NOx Adsorbers: Adsorbate-Controlled Location of Atomically Dispersed Palladium(II) in Ferrierite Determines High Activity and Stability. *Angew. Chem., Int. Ed.* **2022**, *61*, No. e202107554.
(28) Pereira-Hernandez, X. I.; DelaRiva, A.; Kunwar, D.; Xiong, H.; Sudduth, B.; Engelhard, M.; Kovarik, L.; Murayev, V.; Hensen, E.; Wang, Y.; Datye, A. K. Tuning Pt-CeO2 interactions by high-temperature vapor-phase synthesis for improved reducibility of lattice oxygen. *Nat. Commun.* **2019**, *10*, 1358.
(29) Datye, A.; Wang, Y. Atom trapping: a novel approach to generate thermally stable and regenerable single-atom catalysts. *Natl. Sci. Rev.* **2018**, *5*, 630–632.
(30) Jones, J.; Xiong, H.; DeLaRiva, A. T.; Peterson, E. J.; Pham, H.; Challa, S. R.; Qi, G.; Oh, S.; Wiebenga, M. H.; Pereira Hernandez, X. I.; Wang, Y.; Datye, A. K. Thermally stable single-atom platinum-on-ceria catalysts via atom trapping. *Science* **2016**, *353*, 150–154.
(31) Nie, L.; Mei, D.; Xiong, H.; Peng, B.; Ren, Z.; Hernandez, X. I. P.; DeLaRiva, A.; Wang, M.; Engelhard, M. H.; Kovarik, L.; Datye, A. K.; Wang, Y. Activation of surface lattice oxygen in single-atom Pt/CeO2 for low-temperature CO oxidation. *Science* **2017**, *358*, 1419–1423.
(32) Twigg, M. V.; Gandhi, H. Contributions to the Development and Implementation of Catalytic Emissions Control Systems. *Platinum Met. Rev.* **1941-2010**, *2011*, 43–53.
(33) Martienssen, W.; Warlimont, H. *Springer Handbook of Condensed Matter and Materials Data*; Springer, 2005.
(34) Koebel, M.; Elsener, M.; Kleemann, M. Urea-SCR: a promising technique to reduce NOx emissions from automotive diesel engines. *Catal. Today* **2000**, *59*, 335.

https://doi.org/10.1021/jacs.2c09873
J. Am. Chem. Soc. 2023, 145, 5029–5040

(35) Takahashi, N.; et al. The new concept 3-way catalyst for automotive lean-burn engine: NOx storage and reduction catalyst. *Catal. Today* **1996**, *27*, 63.
(36) Koebel, M.; Madia, G.; Elsener, M. Selective catalytic reduction of NO and NO2 at low temperatures. *Catal. Today* **2002**, *73*, 239.
(37) Bourges, P.; Lunati, S.; Mabilon, G. N20 and NO2 formation during NO reduction on precious metal catalysts. *Catalysis And Automotive Pollution Control IV*; Elsevier 1998, *116*, 213.
(38) Kim, C. H.; Qi, G.; Dahlberg, K.; Li, W. N2O and NO2 formation during NO reduction on precious metal catalysts. *Science* **2010**, *327*, 1624−1627.
(39) Harrison, B.; Diwell, A. F.; Hallett, C. Promoting Platinum Metals by Ceria. *Platinum Met. Rev.* **1988**, *32*, 73−83.
(40) Taylor, K. Nitric Oxide Catalysis in Automotive Exhaust Systems. *Catal. Rev.: Sci. Eng.* **1993**, *35*, 457−481.
(41) Granger, P.; Parvulescu, V. I. Catalytic NOx Abatement Systems for Mobile Sources. *Chem. Rev.* **2011**, *111*, 3155−3207.
(42) Khivantsev, K.; Vargas, C.; Tian, J.; Kovarik, L.; Jaegers, N. R.; Szanyi, J.; Wang, Y. Economizing on Precious Metals in Three-Way Catalysts: Thermally Stable and Highly Active Single-Atom Rhodium on Ceria for NO Abatement under Dry and Industrially Relevant Conditions. *Angew. Chem., Int. Ed.* **2021**, *133*, 395−402.
(43) Hadjiivanov, K.; Lavalley, J.-C.; Lamotte, J.; Mauge, F.; SaintJust, J.; Che, M. FTIR Study of CO Interaction with Ru/TiO2Catalysts. *J. Catal.* **1998**, *176*, 415.
(44) Miessner, H. Surface Chemistry in a Zeolite Matrix. Well-Defined Dinitrogen Complexes of Rhodium Supported on Dealuminated Y Zeolite. *J. Am. Chem. Soc.* **1994**, *116*, 11522−11530.
(45) Miessner, H.; Richter, K. Well-defined carbonyl and dinitrogen complexes of ruthenium supported on dealuminated Y zeolite. Analogies and differences to the homogeneous case. *J. Mol. Catal. A: Chem.* **1999**, *146*, 107−115.
(46) Kim, H.; Yang, S.; Lim, Y. H.; Ha, J. M.; Kim, D. H. Upgrading bio-oil model compound over bifunctional Ru/HZSM-5 catalysts in biphasic system: Complete hydrodeoxygenation of vanillin. *J. Hazard. Mater.* **2022**, *423*, No. 126525.
(47) Chakarova, K.; Ivanova, E.; Hadjiivanov, K.; Klissurski, D.; Knozinger, H. Co-ordination chemistry of palladium cations in Pd-H-ZSM-5 as revealed by FTIR spectra of adsorbed and co-adsorbed probe molecules (CO and NO). *Phys. Chem. Chem. Phys.* **2004**, *006*, 3702−3709.
(48) Lee, J.; Kim, J.; Kim, Y.; Hwang, S.; Lee, H.; Kim, C. H.; Kim, D. H. Improving NOx storage and CO oxidation abilities of Pd/SSZ-13 by increasing its hydrophobicity. *Appl. Catal. B: Environ.* **2020**, *277*, No. 119190.
(49) Khivantsev, K., *Selective Synthesis and Characterization of Single-Site HY Zeolite-Supported Rhodium Complexes and Their Use as Catalysts for Ethylene Hydrogenation and Dimerization*; University of South Carolina, Ph.D. Thesis, (2015) (accessed 2022-11-25)
(50) Aitbekova, A.; Wu, L.; Wrasman, C. J.; Boubnov, A.; Hoffman, A. S.; Goodman, E. D.; Bare, S. R.; Cargnello, M. Low-Temperature Restructuring of CeO_2-Supported Ru Nanoparticles Determines Selectivity in CO2 Catalytic Reduction. *J. Am. Chem. Soc.* **2018**, *140*, 13736−13745.
(51) Derk, A. R.; Moore, G. M.; Sharma, S.; McFarland, E. W.; Metiu, H. H Metiu, Catalytic dry reforming of methane on ruthenium-doped ceria and ruthenium supported on ceria. *Top. Catal.* **2014**, *57*, 118−124.
(52) Chester, D.; Derk, A. R.; Sharma, S.; Metiu, H.; McFarland, E. W. CO2 methanation by Ru-doped ceria: the role of the oxidation state of the surface. *Catal. Sci. Technol.* **2015**, *5*, 1783−1791.
(53) Mihaylov, M. Y.; Zdravkova, V. R.; Ivanova, E. Z.; Aleksandrov, H. A.; Petkov, P. S.; Vayssilov, G. N.; Hadjiivanov, K. I. Infrared spectra of surface nitrates: Revision of the current opinions based on the case study of ceria. *J. Catal.* **2021**, *394*, 245−258.
(54) Perdew, J. P.; Chevary, J. A.; Vosko, S. H.; Jackson, K. A.; Pederson, M. R.; Singh, D. J.; Fiolhais, C. Atoms, molecules, solids, and surfaces: Applications of the generalized gradient approximation for exchange and correlation. *Phys. Rev. B* **1992**, *46*, 6671−6687.
(55) Kresse, G.; Hafner, J. Ab initio molecular dynamics for liquid metals. *Phys. Rev. B* **1993**, *47*, 558−561.
(56) *Version VASP.4.9*; http://cms.mpi.univie.ac.at/vasp (accessed 2022-11-25).
(57) Kresse, G.; Joubert, D. From ultrasoft pseudopotentials to the projector augmented-wave method. *Phys. Rev. B* **1999**, *59*, 1758−1775.
(58) Anisimov, V. I.; Aryasetiawan, F.; Lichtenstein, A. I. First-principles calculations of the electronic structure and spectra of strongly correlated systems: the LDA+ U method. *J. Phys.: Condens. Matter* **1997**, *9*, 767−808.
(59) Dudarev, S. L.; Botton, G. A.; Savrasov, S. Y.; Humphreys, C. J.; Sutton, A. P. Electron-Energy-Loss Spectra and the Structural Stability of Nickel Oxide: An LSDA+U Study. *Phys. Rev. B* **1998**, *57*, 1505−1509.
(60) Loschen, C.; Carrasco, J.; Neyman, K. M.; Illas, F. First-principles LDA+U and GGA+U study of cerium oxides. *Phys. Rev. B* **2007**, *75*, No. 035115.
(61) Migani, A.; Vayssilov, G. N.; Bromley, S. T.; Illas, F.; Neyman, K. M. Greatly facilitated oxygen vacancy formation in ceria. *Chem. Commun.* **2010**, *46*, 5936−5938.
(62) Migani, A.; Vayssilov, G. N.; Bromley, S. T.; Illas, F.; Neyman, K. M. Dramatic reduction of the oxygen vacancy formation energy in ceria particles: a possible key to their remarkable reactivity at the nanoscale. *J. Mater. Chem.* **2010**, *20*, 10535−10546.
(63) Aleksandrov, H. A.; Neyman, K. M.; Vayssilov, G. N. The structure and stability of reduced and oxidized mononuclear platinum species on nanostructured ceria from density functional modelling. *Phys. Chem. Chem. Phys.* **2015**, *17*, 14551−14560.
(64) Aleksandrov, H. A.; Neyman, K. M.; Hadjiivanov, K. I.; Vayssilov, G. N. Can the state of platinum species be unambiguously determined by the stretching frequency of an adsorbed CO probe molecule? *Phys. Chem. Chem. Phys.* **2016**, *18*, 22108−22121.
(65) Koleva, I. Z.; Aleksandrov, H. A.; Vayssilov, G. N. Decomposition behavior of platinum clusters supported on ceria and γ-alumina in the presence of carbon monoxide. *Catal. Sci. Technol.* **2017**, *7*, 734−742.
(66) Vayssilov, G. N.; Lykhach, Y.; Migani, A.; Staudt, T.; Petrova, G. P.; Tsud, N.; Skála, T.; Bruix, A.; Illas, F.; Prince, K. C.; Neyman, K. M.; Libuda, J. Support nanostructure boosts oxygen transfer to catalytically active platinum nanoparticles. *Nat. Mater.* **2011**, *10*, 310−315.
(67) Lee, J.; Ryou, Y. S.; Chan, X.; Kim, T. J.; Kim, D. H. How Pt Interacts with CeO2 under the Reducing and Oxidizing Environments at Elevated Temperature: The Origin of Improved Thermal Stability of Pt/CeO2 Compared to CeO2. *J. Phys. Chem. C* **2016**, *120*, 25870−25879.
(68) Alcala, R.; DeLaRiva, A.; Peterson, E. J.; Benavidez, A.; Garcia-Vargas, C.; Benavidez, A.; Jiang, D.; Pereira-Hernández, X. I.; Brongersma, H. H.; Veen, R.; Staněk, J.; Miller, J. T.; Wang, Y.; Datye, A. Atomically Dispersed Dopants for Stabilizing Ceria Surface Area. *Appl. Catal. B Environ.* **2021**, *284*, No. 119722.
(69) Klimisch, R.L.; Larson, J.G., *The Catalytic Chemistry of Nitrogen Oxides*; Plenum Press: New York (1975).
(70) Kim, J. H.; Yoon, S.; Baek, D. S.; Kim, J.; Kim, J.; An, K.; Joo, S. H. Boosting Thermal Stability of Volatile Os Catalysts by Downsizing to Atomically Dispersed Species. *JACS Au* **2022**, *2*, 1811−1817.
(71) Narula, C. K.; Allard, L. F.; Stocks, G. M.; Moses-DeBusk, M. Remarkable NO oxidation on single supported platinum atoms. *Sci. Rep.* **2014**, *4*, 7238.
(72) Narula, C. K.; Allard, L. F.; Moses-DeBusk, M.; et al. Single Pd Atoms on θ-Al_2O_3 (010) Surface do not Catalyze NO Oxidation. *Sci. Rep.* **2017**, *7*, 560.
(73) Toso, A.; Danielis, M.; de Leitenburg, C.; Boaro, M.; Trovarelli, A.; Collussi, S. Key Properties and Parameters of Pd/CeO2 Passive NOx Adsorbers. *Ind. Eng. Chem. Res.* **2022**, *61*, 3329−3341.
(74) Ryou, Y. S.; Lee, J.; Lee, H.; Kim, C. H.; Kim, D. H. Low temperature NO adsorption over hydrothermally aged Pd/CeO2 for cold start application. *Catal. Today* **2018**, *307*, 93−101.

https://doi.org/10.1021/jacs.2c09873
J. Am. Chem. Soc. 2023, 145, 5029−5040

(75) Ji, Y.; Xu, D.; Bai, S.; Graham, U.; Crocker, M.; Chen, B.; Shi, C.; Harris, D.; Scapens, D.; Darab, J. Pt- and Pd-Promoted CeO2−ZrO2 for Passive NOx Adsorber Applications. *Ind. Eng. Chem. Res.* **2017**, *56*, 111−125.
(76) Hong, Z.; Wang, Z.; Li, X. Catalytic oxidation of nitric oxide (NO) over different catalysts: an overview. *Catal. Sci. Technol.* **2017**, *7*, 3440−3452.
(77) Zhang, L.; Spezzati, G.; Muravev, V.; Verheijen, M. A.; Zijlstra, B.; Filot, I. A. W.; Su, Y.-Q.; Chang, M.-W.; Hensen, E. J. M. Improved Pd/CeO2 Catalysts for Low-Temperature NO Reduction: Activation of CeO2 Lattice Oxygen by Fe Doping. *ACS Catal.* **2021**, *11*, 5614−5627.
(78) Srinivasan, P. D.; Khivantsev, K.; Tengco, J.; Zhu, H.; Bravo-Suárez, J. J. Enhanced Ethanol Dehydration on gamma-Al2O3 Supported Cobalt Catalyst. *J. Catal.* **2019**, *373*, 276−296.
(79) Müller, P.; Hermans, I. Applications of Modulation Excitation Spectroscopy in Heterogeneous Catalysis. *Ind. Eng. Chem. Res.* **2017**, *56*, 1123−1136.
(80) Ferri, D.; Kumar, M. S.; Wirz, R.; Eyssler, A.; Korsak, O.; Hug, P.; Weidenkaff, A.; Newton, M. A. Newton, First steps in combining modulation excitation spectroscopy with synchronous dispersive EXAFS/DRIFTS/mass spectrometry for in situ time resolved study of heterogeneous catalysts. *Phys. Chem. Chem. Phys.* **2010**, *12*, 5634−5646.

https://doi.org/10.1021/jacs.2c09873
J. Am. Chem. Soc. 2023, 145, 5029−5040